Orientation Distribution Functions Obtained via Polarized Raman Spectroscopy of Poly(ethylene terephthalate) Fibers

Shuying Yang† and Stephen Michielsen*

School of Polymer, Textile and Fiber Engineering, Georgia Institute of Technology, Atlanta, Georgia 30332-0295

Received April 15, 2003; Revised Manuscript Received May 21, 2003

ABSTRACT: Polarized Raman microspectroscopy was used to analyze uniaxially oriented fibers of poly(ethylene terephthalate) (PET). A full analysis of bands at 1616, 998, and 1096 cm^{-1} is reported for cylindrically symmetric PET fibers. Average orientation and crystal orientation are obtained from the 1616 and 998 cm^{-1} band, respectively. Although both the 1096 and the 998 cm^{-1} bands are related to the crystallinity, the second Legendre polynomial of the 1096 cm^{-1} band, $P_{2,1096}$, is substantially smaller than for the 998 cm^{-1} band, $P_{2,998}$. In addition, $P_{2,1096}$ is not related to the birefringence of the samples, and there is no simple relationship between $P_{2,1096}$ and $P_{2,998}$. The orientation distribution functions (ODFs) for these vibrations were obtained by assuming a Gaussian distribution with a tilt angle relative to the fiber axis and specific to each vibration. The 1616 cm^{-1} band has a tilt angle of 23 ± 4°, and the ODF becomes narrower as molecular orientation increases. The 998 cm^{-1} band has a tilt angle of approximately 0°, and the ODF is always very narrow. On the other hand, the tilt angle of the 1096 cm^{-1} band increases, and the ODF becomes narrower as the molecular orientation increases. However, because of the large tilt angle, P_2 for this band *decreases* as the molecular orientation *increases*.

Introduction

PET is a semicrystalline polymer with crystallinity ranging from 0 to about 60%. It is widely used to produce fibers, films, and containers. PET's physical properties depend strongly on the morphology (orientation and crystallinity). Many techniques such as infrared dichroism, polarized Raman spectroscopy, polarized fluorescence, NMR, interference microscopy, and X-ray diffraction have been used to characterize the orientation of the polymer chains. Among them, polarized Raman microscopy is unique in that it can provide both the second- and fourth-order Legendre polynomials, P_2 and P_4, for particular *vibrations* within the samples. P_2 and P_4 are given explicitly in the theoretical section below. Since Bower[1] developed the theory and the procedures for determining the orientation of polymer samples by polarized Raman spectroscopy in 1972, several studies have been performed on PET samples.[2−10] These studies found that vibrational bands 1616 and 631 cm^{-1} are related to the benzene ring in PET. The 1616 cm^{-1} band has been assigned to the symmetric stretching of the 1,4-carbons of the benzene ring[2] and is believed to provide the average molecular orientation of the polymer chains.[2,5,11]

The 998 cm^{-1} region has been assigned to three different bands. The 1030 cm^{-1} band is associated with the gauche configuration of the ethylene glycol unit of PET. The 993 cm^{-1} band has been assigned to the symmetric stretching of the O−CH_2 bond and the stretching of the C−C bond in ethylene glycol units of all-trans configuration[12−15] in the *noncrystalline* region. The 998 cm^{-1} band has been assigned to the same vibration in the *crystalline* region. When studying spin-oriented and drawn fibers of PET, Adar and Noether[16] noticed that fibers spun at low take-up speeds consistently exhibited a weak peak at about 1030 cm^{-1}; as the take-up speed was increased, the weak band at 1030 cm^{-1} was replaced by a well-defined, relatively sharp band at 998 cm^{-1}. We observed the same phenomena.

Boerio and Bahl[12] attributed the band at 1096 cm^{-1} to the combined vibration of benzene ring CC stretching, CC stretching in the ethylene glycol unit, and ester C(O)−O stretching. Stokr et al.[13] and Quintanilla et al.[15] observed that the 1096 cm^{-1} band intensity increased with annealing of the samples. According to Stokr et al., this band is characteristic of tTt conformations in the chain, which is the form found in the crystalline phase of PET. In this structure, t refers to the trans conformation about the O−C axis of the glycol unit and T refers to the trans conformation about the C−C axis of the ethylene unit. Ellis et al.[17] reported that the intensity of this band increases with the degree of extension induced in the PET samples. Adar and Noether[18] found this band in the crystallized PET samples. The intensity of the 1096 cm^{-1} band has been shown to correlate with the full width at half-maximum of the 1725 cm^{-1} band, $fwhm_{1725}$, and the sample density or crystallinity.[14,17,19] The relative intensity of this band correlates linearly with the sample density. However, no complete analysis of the orientation of this band appears in the literature.

Although Bower[1] had shown that the three principal components of the Raman tensor and the second- and fourth-order Legendre polynomials, P_2 and P_4, could be determined directly from the Raman spectra for cylindrically symmetric samples, the early studies did not use the full analysis. They made what appeared to be reasonable assumptions, namely that the Raman tensor ratios of the particular vibrations were insensitive to the local environment and the Raman tensor of the vibration was cylindrically symmetric. This allowed the Raman tensor ratio, r, to be determined from isotropic samples.[2,3,6] This assumption implies that the Raman

* Corresponding author. E-mail Stephen.michielsen@tfe.gatech.edu.
† Current address: Mechanical Engineering Department, University of Texas Pan American, Edinburg, TX 78539.

10.1021/ma034486q CCC: $25.00
Published on Web 07/17/2003

tensor does not change with morphology (crystallinity and/or orientation). This reduced the number of unknowns from 5 to 3, which could be determined from the Raman spectra of the samples in three convenient experimental geometries.

However, in 1995, Citra et al.[20] showed that the principal components of the Raman tensor in polyethylene changed with morphology, and thus the assumption that they were constant was invalid. Later, Lesko et al.[11] measured the Raman spectra of the 1616 cm^{-1} band in PET fibers in 12 different geometries to obtain the five normalized spectra needed to determine the three Raman tensor principal components α_1, α_2, and α_3 and two orientation parameters P_2 and P_4. The additional spectra were obtained to help to normalize the intensities of the spectra from the different geometries. They found that, not only did P_2 and P_4 change with morphology, as expected, but that the principal components of the Raman tensor also changed, confirming the observation by Citra et al. The results presented by Lesko et al. will be compared with those of the current study in the Results section.

Recently, Yang and Michielsen[21] performed the full Raman analysis on the 998 cm^{-1} band. They found that this band could be used to determine the orientation of the crystalline region in their samples, and it was independent of the sample birefringence. At low birefringence, they noted that this band occurred at 993 cm^{-1} and thus indicated that the all-trans glycol unit existed primarily in the noncrystalline region, while at high orientation, they existed primarily in the crystalline region.

In an attempt to verify the work of Lesko et al. and to extend the work of Yang and Michielsen, a detailed analysis of the 1616, 998, and 1096 cm^{-1} Raman bands for cylindrically symmetric PET fibers is presented below.

Theory

The theory for calculating the orientation parameters of fiber symmetry by Raman spectroscopy has been derived explicitly by Bower[1] and summarized by Citra et al.[20] Yang and Michielsen[21] provided a simplified version, which is repeated below:

$$I_{33}^{BS}(0) = 3_{\bar{2}(33)2} = K(A - 2BP_2 + CP_4)$$

$$I_{33}^{BS}(90) = I_{11}^{BS}(0) = 1_{\bar{2}(33)2} = K(A + BP_2 + 3CP_4/8)$$

$$I_{31}^{BS}(0) = 3_{\bar{2}(31)2} = K(D - EP_2 - {}^1/_2CP_4)$$

$$I_{21}^{RAS}(0) = 3_{1(21)2} = K(D + EP_2 + CP_4/8)$$

$$I_{31}^{BS}(45) = (31\text{-plane}, \angle 45° \text{ to } 3)_{\bar{2}(31)2} = K(D - {}^1/_2EP_2 + 19CP_4/32) \quad (1)$$

where the $I_{xy}^{configuration}(\#)$ is the scattered intensity in the backscattering configuration, BS, or right angle scattering, RAS, with the laser polarization in the x direction and the analyzer polarized in the y direction. The number in parentheses indicates the angle between the long axis of the fiber and the laboratory 3-axis. The fiber lies in the 31-plane. In our apparatus, the laser polarization is always in the 3-direction when using the backscattering configuration. From symmetry, we obtain $I_{11}^{BS}(0)$, which is just equal to $I_{33}^{BS}(90)$. An alternative nomenclature is provided as a modified Porto nomenclature,[22] $i_{j(kl)m}$, where the nonsubscripted number, e.g. i, specifies the orientation of the long axis of the fiber. The subscript is the normal Porto system where the first number, j, is the propagation direction of the laser, the second number is the laser polarization direction, the third number is the polarization direction of the analyzer, and the fourth number is the propagation direction of the scattered light. $A-E$ are functions of α_1/α_3 and α_2/α_3 only, where α_1, α_2, and α_3 are the principal components of the Raman tensor as given by Yang and Michielsen.[21] $K = I_0N_0\alpha_3^2$, where I_0 is the incident intensity and N_0 is the number of scatterers within the scattering volume. P_2 and P_4 are the average values of the second- and fourth-order Legendre polynomials, respectively:

Table 1. Sample Processing Conditions and Sample Properties

sample	spinning speed (m/min)	draw ratio	density (g/mL)	birefringence	crystallinity
S_15	1463		1.341	0.014	0.05
S_20	2012		1.344	0.018	0.08
S_25	2469		1.344	0.024	0.08
S_32	3200		1.345	0.045	0.08
S_41	4115		1.355	0.069	0.17
S_41_HMW	4115		1.363	0.078	0.23
D_20_0	2000		1.343	0.020	0.07
D_*x*	*a*	*a*	1.368	0.095	0.28
D_30_24	3000	2.4	1.397	0.187	0.52
D_45_19	4500	1.9	1.396	0.194	0.51

[a] Unknown.

$$P_2 = \langle P_2(\cos\theta)\rangle = (3\langle\cos^2\theta\rangle - 1)/2$$

$$P_4 = \langle P_4(\cos\theta)\rangle = (35\langle\cos^4\theta\rangle - 30\langle\cos^2\theta\rangle + 3)/8 \quad (2)$$

where the angle brackets, $\langle\ \rangle$, indicate the average is taken over all chain segments within the scattering volume. The angle θ is the angle between the Raman tensor principal component α_3 and the long axis of the fiber.

From symmetry, $I_{31} = I_{13} = I_{32} = I_{23}$ and $I_{11} = I_{22}$. These relationships can be used to normalize scattered intensities from different experimental configurations and geometries.

Experiment

Two sample sets were analyzed (Table 1). The first set was provided by DuPont and consisted of fibers prepared at spinning speeds of 1463−4115 m/min, the "S" series. Two of these samples were spun under identical conditions at 4115 m/min, but one had a higher molecular weight (S_41_HMW) than the other. The second set consisted of four samples spun at various speeds, drawn under various conditions and annealed under tension at 150 °C in a continuous draw−anneal process, the "D" series. Annealing times were less than 1 s.

Single filaments of each of these samples were extracted and glued across the opening of $^1/_4$-in. (~6 mm) steel washers. The Raman spectra were obtained on a Holoprobe Research 785 Raman microscope made by Kaiser Optical Systems, Inc., using a 10× objective. Approximately 3 mW of 785 nm laser light was focused onto the filaments in the region of the opening in the washer. Polarized Raman spectra were collected in all five geometries and polarizations, $I_{33}^{BS}(0)$, $I_{33}^{BS}(90)$, $I_{31}^{BS}(0)$, $I_{21}^{RAS}(0)$, $I_{31}^{BS}(45)$. Two additional, degenerate spectra, $I_{23}^{RAS}(0)$ and $I_{31}^{BS}(90)$, were obtained to normalize the $I_{21}^{RAS}(0)$ and the $I_{33}^{BS}(90)$ spectra to the I_{33} spectra. Three specimens were used from each sample.

All data acquisition was performed using the Kaiser Optical Systems' "HoloGRAMS" software and analyzed using the GRAMS32 software package (Galactic Industries Inc.) The imbedded curve-fit routine was used to obtain the center, height, full width at half-maximum (fwhm), and the Gaussian and Lorentzian content for each peak. The area under the peak was taken as the intensity of the peak. The detailed experimental setup and data analysis have been published previously.[21,23]

Results and Discussion

Since the samples used in the current study were the same ones used by Natarajan and Michielsen[22,24] to develop correlations between the birefringence and Lorentz density with the Raman spectra, the birefringence, Δn, and the Lorentz densities, ρ, were determined by applying the functions developed previously:

$$\Delta n = 0.001 + 0.0267(I_{33,998}/I_{33,702}) + 0.00047(I_{33,1616}/I_{33,702})^2 \quad (3)$$

$$\rho = 1.402 + 0.00177(I_{33,998}/I_{33,702}) - 0.024(FWHM_{33,1725}) + 0.00083(I_{33,998}/I_{33,702})^2 \quad (4)$$

where $I_{33,x}$ is the $I_{33}^{BS}(0)$ intensity of the x cm^{-1} Raman band and fwhm$_{33,1725}$ is the full width at half-maximum of the $I_{33}^{BS}(0)$ intensity of the 1725 cm^{-1} Raman band. These are shown in Table 1, along with the crystallinity, X_c, which was determined from the density:

$$X_c = (\rho - \rho_a)/(\rho_c - \rho_a) \quad (5)$$

where ρ is obtained from eq 4, $\rho_a = 1.335$ g/cm^3 is the density of the purely amorphous phase, and $\rho_c = 1.455$ g/cm^3 is the density of the pure crystalline phase.[25] In addition, Herman's orientation function, which is just the second-order Legendre polynomial, P_2, for the chain was determined using the analysis by Kashiwagi et al.:[2,22,24]

$$P_{2,\Delta n} = \Delta n/\Delta n_{max} \quad (6)$$

where the subscript "Δn" refers to P_2 obtained from birefringence from eq 3 and Δn_{max} is the maximum birefringence for the fully oriented chains. For PET, $\Delta n_{max} = 0.245$[2].

The intensities of the depolarized spectra were corrected for the depolarization ratio of the Raman instrument, instrumental factor, as previously described.[21,23] Briefly, it was found that the instrumental factor decreases with the increase of wavenumber in the Raman shift. The depolarization ratio for chemicals with known depolarization ratios for specific bands, butyl benzoate, 2-butanone, CCl_4, and amorphous PET, were determined. The instrumental factor, $F(\nu)$, was determined:

$$F(\nu) = \text{known depolarization ratio}/\text{measured depolarization ratio} \quad (7)$$

The intensities for the depolarized spectra were then multiplied by the instrumental factor to obtain the corrected intensity:

$$I_{x\neq y}^{corr} = F(\nu) I_{x\neq y}^{measured} \quad (8)$$

In addition, since the intensities given in eq 1 are absolute intensities, the spectra from the different geometries need to be corrected for differences in focus and laser power. This was accomplished by using the symmetry relationships $I_{31} = I_{13} = I_{32} = I_{23}$, $I_{33}^{BS}(90) = I_{11}^{BS}(0)$, and $I_{31}^{BS}(90) = I_{13}^{BS}(0)$. Thus

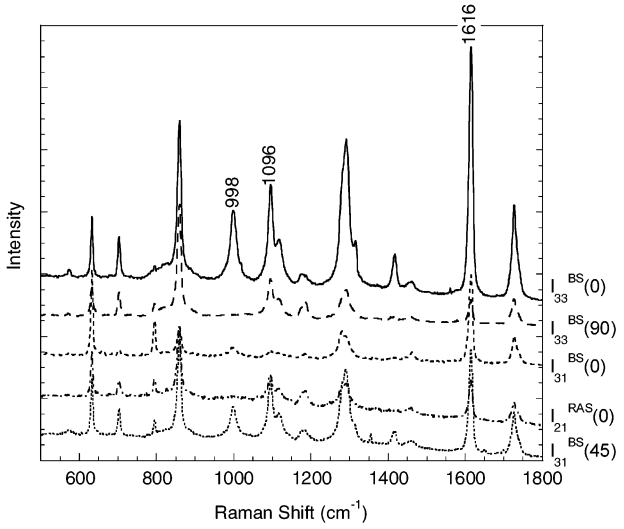

Figure 1. Five uncorrected, unique Raman spectra for sample D_30_24 are shown in the range 500−1800 cm^{-1}. The three bands discussed in this paper are labeled.

$$I_{33}^{BS}(0)^{true} = I_{33}^{BS}(0)^{meas}$$

$$I_{11}^{BS}(0)^{true} = I_{31}^{BS}(0)^{meas} I_{33}^{BS}(90)^{meas}/I_{31}^{BS}(90)^{meas}$$

$$I_{31}^{BS}(0)^{true} = F(\nu) I_{31}^{BS}(0)^{meas}$$

$$I_{21}^{RAS}(0)^{true} = F(\nu) I_{31}^{BS}(0)^{meas} I_{21}^{RAS}(0)^{meas}/I_{23}^{RAS}(0)^{meas}$$

$$I_{31}^{BS}(45)^{approx} = F(\nu) I_{31}^{BS}(45)^{meas} \quad (9)$$

The superscripts "meas", "true", and "approx" refer to the measured, true, and approximately true intensities, respectively. $I_{31}^{BS}(45)^{approx}$ was used rather than $I_{31}^{BS}(45)^{true}$ because (a) there was no simple relationship to use for correction and (b) it was found that the correction due to $I_{31}^{BS}(0)^{meas}/I_{31}^{BS}(90)^{meas}$ was always less than 10% and usually less than 5% provided that these spectra were obtained by first recording the $I_{31}^{BS}(0)$ spectra, then rotating the fiber in the 31-plane such that the fiber long axis made a 45° angle with the 3-axis, refocusing, and collecting the $I_{31}^{BS}(45)$ spectra. Next, the fiber was again rotated in the 31-plane until the fiber long axis made a 90° angle with the 3-axis, refocusing, and collecting the $I_{31}(90)$ spectra. The correction to $I_{31}^{BS}(45)^{meas}$ should be no greater than for $I_{33}^{BS}(90)^{meas}$, i.e., less than 5−10%, and thus is insignificant. The spectra were always recorded in this sequence. The good agreement between P_2, P_4, α_1/α_3, α_2/α_3, and α_3^2 of the current study and that of Lesko et al.[11] as discussed below and as shown in Figures 2 and 6 indicates that this correction is adequate. The uncorrected spectra are shown in Figure 1 for sample D_30_24.

Analysis of the 1616 cm^{-1} Region. The Raman spectra of each specimen were obtained as described in the Experimental Section. From Figure 1, it is clear that $I_{33}^{BS}(0) \neq I_{33}^{BS}(90)$, indicating a highly ordered sample.

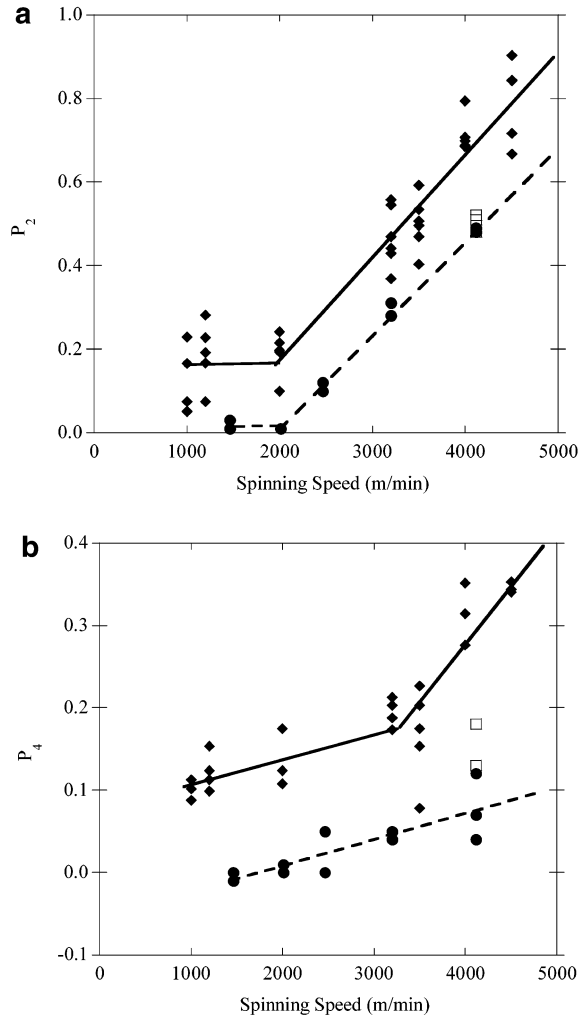

Figure 2. (a) P_2 and (b) P_4 for the 1616 cm^{-1} band: ◆ are from Lesko et al.,[11] ● are from this study, and □ are for the high molecular weight sample in this study.

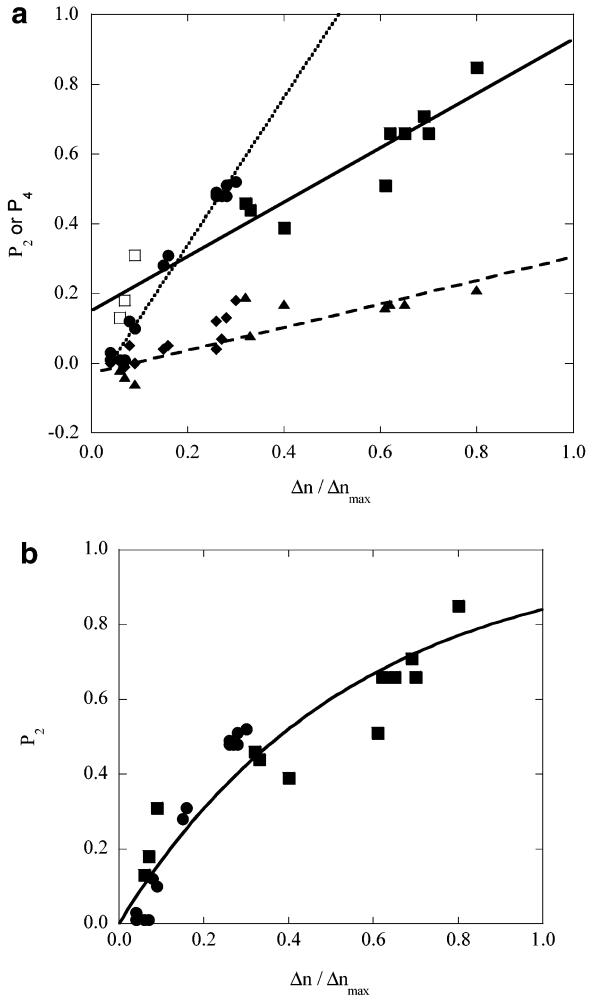

Figure 3. (a) P_2 and P_4 for the 1616 cm^{-1} band vs birefringence and (b) P_2 replotted with the curve representing eq 11. ■ are for P_2 from drawn and annealed series, □ are P_2 of sample D_20_0, which was undrawn, ● are for P_2 from spin speed series, ▲ are for P_4 from drawn and annealed series, and ◆ are for P_4 from spin speed series. Lines are linear regressions for P_2 of drawn and annealed samples, solid, P_4 of drawn and annealed samples; dashed, P_2 of spin speed series, dotted.

The intensities of the 1616 cm^{-1} band were obtained via curve fitting also described in the Experimental Section. After making the above corrections to the measured intensities, the true intensities were substituted into eqs 1 and solved simultaneously using Mathematica (Wolfram Research, Inc.) to obtain the five unknown values, P_2, P_4, $a_1 = \alpha_1/\alpha_3$, $a_2 = \alpha_2/\alpha_3$, and $K = I_0 N_0 \alpha_3^2$. P_2 and P_4 for spin series samples (S_15−S_41_HMW) are shown in Figure 2 along with the results by Lesko et al.[11] P_2 follows the same trend in the present study as in that of Lesko et al., although our values of P_2 are approximately 0.15 lower than theirs. Both sets exhibit a sharp break at 2000 m/min. At lower speeds, P_2 is nearly independent of spinning speed, while at higher speeds, P_2 depends strongly on spinning speed. In our study the value of P_2 does not seem to be sensitive to the molecular weight.

Lesko et al. attributed the sharp break in their P_2 and P_4 curves as being due to the sudden increase in oriented amorphous regions and the onset of crystallization. Our values of P_2 exhibit a break in the curve at exactly the same speed as theirs, indicating a similar process. It is also clear that our values of P_4 are lower than those of Lesko et al. More importantly, there is no break in the dependence of P_4 on spinning speed in our study while there is a sharp break at 3000 m/min in their study (see Figure 2b). The higher molecular weight sample in our study has a much higher value of P_4 than the lower molecular weight sample. This may help explain the differences between the two studies. If their sample were spun at a lower temperature or with higher molecular weight polymer than ours, the viscosity would be higher for their samples than ours, resulting in a more highly oriented sample, as indicated by the higher values of P_2 and P_4 observed by Lesko et al.[11]

In addition to the spin speed series, we also determined P_2 and P_4 for samples that had been drawn and annealed. The results of P_2 and P_4 for all of our samples are shown in Figure 3a plotted against the birefringence. It appears that P_2 depends linearly on the birefringence, although the spin speed series, S-series, has a different dependence than the drawn and annealed series, D-series. The three open squares correspond to three specimen from a single sample that was spun at 2000 m/min but that was neither drawn nor annealed. These data could be fit by either of the two P_2 lines. However, both of these lines extrapolate to unreasonable values. The dotted line extrapolates to a value of $P_2 > 1$ for $\Delta n/\Delta n_{max} > 0.55$, but P_2 must be less than or equal to 1. The solid line extrapolates to

$\sim$0.16 for $\Delta n/\Delta n_{max} = 0$. However, $\Delta n/\Delta n_{max} = 0$ indicates a randomly oriented sample for which P_2 must equal 0. In addition, Purvis and Bower[3] state that the α_3 principal component axis lies along the C_1-C_4 axis of the phenyl ring and that the C_1-C_4 axis of the phenyl ring is calculated to lie at 19°12′ to the chain axis. Using their analysis and the Legendre polynomial identity

$$P_2(1616) = P_2(C_1\text{-}C_4) = P_2(\alpha_3) = P_2(\text{chain})P_2(19°12') \quad (10)$$

and that $P_2(\text{chain}) = P_{2,\Delta n} = \Delta n/\Delta n_{max} \leq 1.0$, so that the maximum value of $P_2(\alpha_3)$ is 0.841, which is below the value of $P_2(\alpha_3)$ obtained from the extrapolation of the solid line to $\Delta n/\Delta n_{max} = 1.0$. Curves other than a straight line can be fit to these data. We suggest

$$P_2(\alpha_3) = 1 - \exp(-1.84P_{2,\Delta n}) \quad (11)$$

which fits the data of all of the samples used in the current study, has the correct asymptotic dependence, and is shown in Figure 3b. This implies that at low overall chain orientation (low $P_{2,\Delta n}$) the α_3 axis, which is believed to be collinear with the C_1-C_4 axis, can line up easily with the fiber axis; i.e., $P_2(1616)$ increases rapidly. As the chain orientation increases, the C_1-C_4 axis must rotate toward 19°, and thus the rate of increase in $P_2(1616)$ must decrease until at perfect chain alignment $P_2(1616) = 0.841$.

Figure 3a also shows that $P_4(1616)$ increases linearly with $P_{2,\Delta n} = \Delta n/\Delta n_{max}$. However, the scatter in the data is too large to exclude other functional dependencies on $P_{2,\Delta n}$. Since P_4 is a higher moment of the orientation distribution function than P_2, there is no reason to expect any particular functional dependence of P_4 on $P_{2,\Delta n}$.

Further analysis of P_2 and P_4 using eqs 2 yields the average values of $\cos^2\theta$ and $\cos^4\theta$. The average value of $\cos^{2n}\theta$ is given by

$$\langle\cos^{2n}\theta\rangle = \int_0^{\pi/2} 2\pi w(\theta)\cos^{2n}\theta\sin\theta\,d\theta \Big/ \int_0^{\pi/2} 2\pi w(\theta)\sin\theta\,d\theta \quad (12)$$

where $w(\theta)$ is the weighting function for the distribution. By assuming a Gaussian weighting function with an angular offset relative to the fiber axis, ϕ

$$w(\theta) = \exp(-m[\theta - \phi]^2) \quad (13)$$

where m is the Gaussian factor, the orientation distribution function for the α_3 axis can be determined. We minimized the sum $[P_2(\text{fit}) - P_2(\text{experiment})]^2 + [P_4(\text{fit}) - P_4(\text{experiment})]^2$, where $P_{2n}(\text{fit})$ are obtained for P_2 and P_4 from eqs 2 using eqs 12 and 13 to obtain m and ϕ. $P_{2n}(\text{experiment})$ are just the values we obtained by solving eqs 1 using the corrected intensities from our spectra. For this fitting, we used the "Solver" routine in Microsoft Excel. The orientation distribution function (ODF) is shown in Figure 4 for low-, medium-, and high-birefringence specimen. At low birefringence, the ODF is nearly flat, extending over all angles. As the orientation increases, initially the ODF peaks at $\phi = 0°$. However, as the orientation increases further and with the onset of crystallinity, the offset angle ϕ rotates from 0 to 23 ± 4°. This indicates that for highly oriented and crystallized specimen ϕ is close to the predicted value of 19° used by Purvis and Bower.[3] Using the crystal structure given by Daubeny and Bunn,[26] the C_1-C_4 axis is calculated to lie at 23° to the crystal axis, in agreement with the findings from Figure 3b described above. In other words, the α_3 axis lies very close to the C_1-C_4 axis.

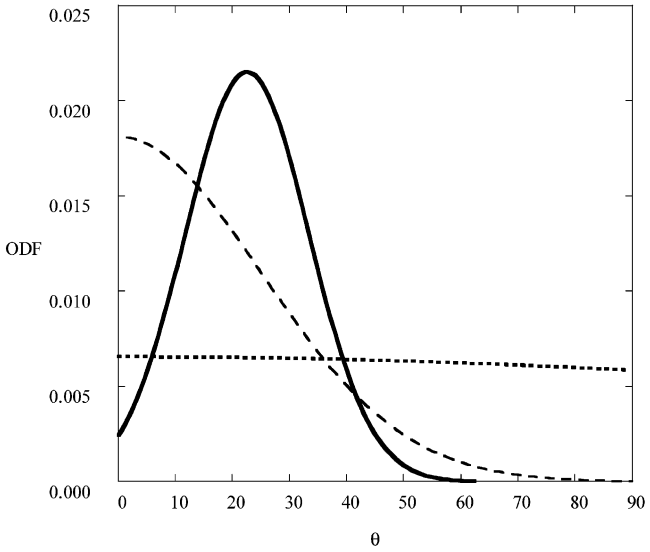

Figure 4. Distribution of θ obtained by fitting eqs 12 and 13 to the measured values of P_2 and P_4 for the 1616 cm^{-1} Raman band of sample S_15, dotted curve, S_41, dashed curve, and D_30_24, solid curve.

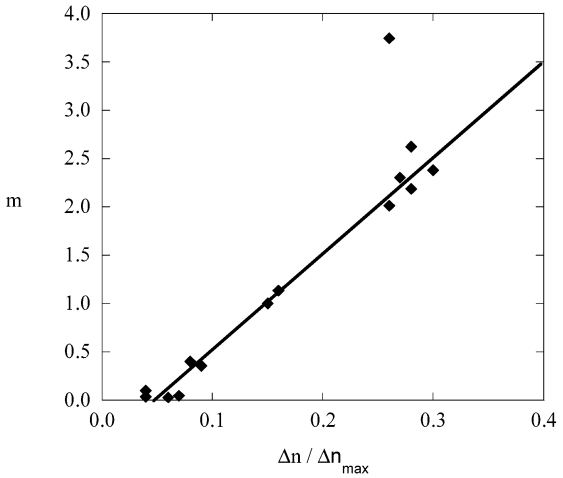

Figure 5. Values of m obtained from eq 13 vs birefringence for the S-series. Line is linear regression for all points except the one apparent outlier.

The values of m obtained from eq 13 are shown in Figure 5 for the S-series. For this series, m is seen to depend linearly on the birefringence. From statistics, for a Gaussian distribution, the full width at half-maximum, fwhm, = 1.1774/m. Thus, as birefringence increases, the width of the orientation distribution function decreases.

Finally, Lesko et al.[11] found that the Raman tensor ratios a_1 and a_2 as well as the tensor component α_3^2 varied with spinning speed. Figure 6a shows a_1 and a_2 from our experiments and from Lesko et al. Clearly, the trends for a_1 and a_2 in both our work and that of Lesko et al. are the same. a_1 and a_2 are of opposite sign, a_1 decreases, and a_2 increases with spinning speed until they reach plateaus near 2500 m/min. In Lesko et al., they also display their value of $\beta = I_0N_0\alpha_3^2$ (their Figure 9). However, they do not describe how they obtained β.

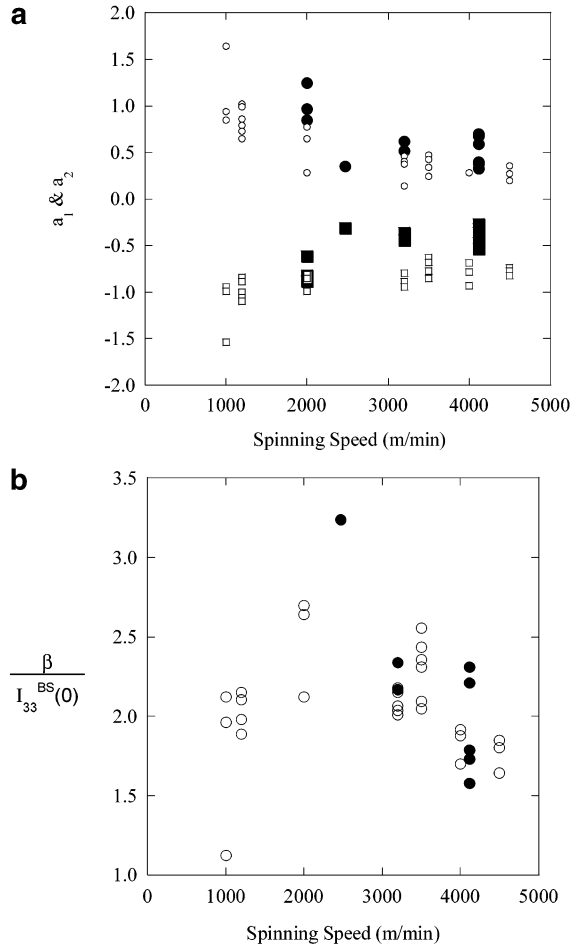

Figure 6. (a) Dependence of a_1, circles, and a_2, squares, and (b) dependence of β (Lesko et al.) or K (this paper) normalized by $I_{33}^{BS}(0)$ are plotted against the spinning speed. Open symbols are from Lesko et al. while filled symbols are from our experiments.

In a previous paper by the same group, they appear to normalize their intensity data by dividing all intensities by $I_{33}^{BS}(0)$, although they do not discuss this normalization. (see Table 1 of ref 20.) In Figure 6b we plot $I_0 N_0 \alpha_3^2 / I_{33}^{BS}(0) = K/I_{33}^{BS}(0)$ along with their data for "β", which we believe has been normalized in the same way. Clearly, there is good agreement between our values and theirs in the range of spinning speeds from 3000 to 4200 m/min.

Both a_1 and a_2 are shown in Figure 7a as functions of the crystallinity. a_1 decreases with increasing density until it reaches a value of 0.3 at a density of 1.37 g/mL, while a_2 increases with increasing density until it reaches a value of -0.3, also at a density of 1.37 g/mL or at a crystallinity of 0.29. Figure 7b shows the value of α_3^2 times an arbitrary constant, κ, as a function of crystallinity. [$\kappa \neq I_{33}^{BS}(0)$. We chose this form to avoid any dependence of $I_{33}^{BS}(0)$ on morphology.] α_3^2 increases rapidly with crystallinity up to $X_c = 0.37$ or a density of 1.38 g/mL. Thereafter, α_3^2 remains constant. This indicates that, as the chain segments get closer together and as they are incorporated into the crystalline phase, the local field effects asymptotically approach constant values. In the limit of a perfect crystal, we would expect all of the local field effects to be identical, and thus a_1, a_2, and α_3^2 should become constant, which is consistent with our data.

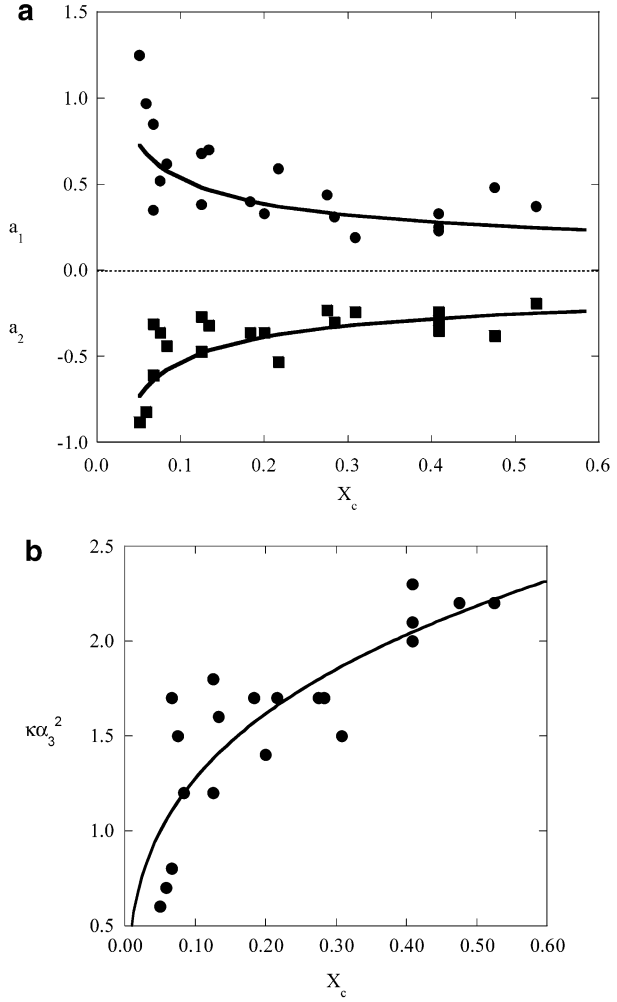

Figure 7. (a) Ratio of the principal Raman tensor components $a_1 = \alpha_1/\alpha_3$ (●) and $a_2 = \alpha_2/\alpha_3$ (■) and (b) the principal Raman tensor component α_3^2 of the 1616 cm^{-1} Raman band are shown plotted as functions of the crystallinity. κ is an arbitrary constant that accounts for the number of scatterers, the laser intensity, and instrumental factors.

Analysis of the 998 cm^{-1} Region. The 998 cm^{-1} region consists of three bands. The 993 cm^{-1} band has been assigned to the symmetric stretching of the O−CH_2 bond and the stretching of the C−C bond in the ethylene glycol units of all-trans conformations (O−C, C−C, and O−C all in the trans configuration) in the noncrystalline region, the 998 cm^{-1} band has been assigned to the same conformation in the crystalline region, and the 1030 cm^{-1} band has been assigned to the gauche conformation of the ethylene glycol unit in the noncrystalline region.[13] The analysis of the postdrawn series (D-series) has been published elsewhere.[21] Here we report the combined results for both the D-series and the S-series.

As shown in Figure 8, sample S_15 exhibits only one peak, a very broad band centered at 1030 cm^{-1}. This band has a Gaussian shape, which is consistent with it being a Raman band from the amorphous region where the local field effects should be random. Likewise, sample D_30_24 has a single band at 998 cm^{-1}. This band has a Lorentzian shape, which is consistent with the assignment to a Raman band in the crystalline region where the local field effects are expected to be uniform. On the other hand, sample S_32 exhibits three bands—one at 1030 cm^{-1} and two overlapped bands at 993 and 998 cm^{-1}. This sample has moderate orienta-

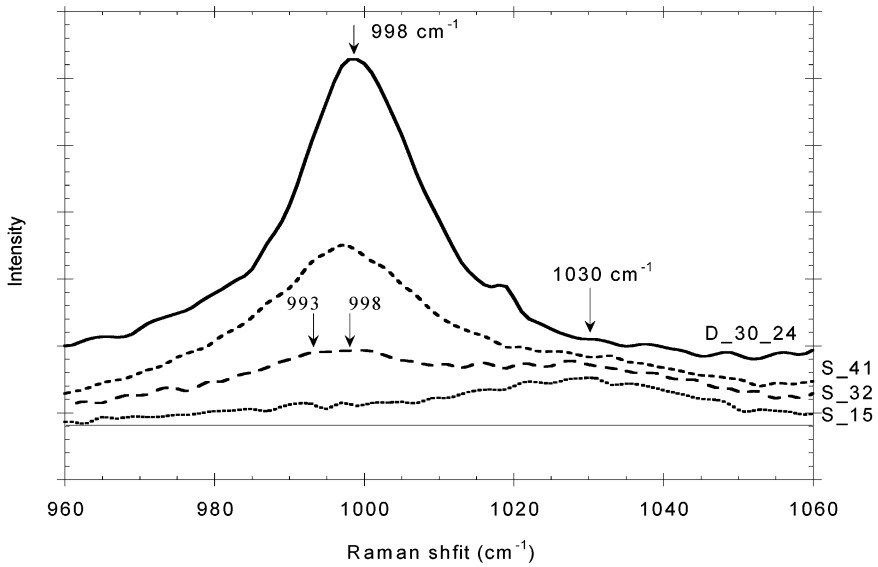

Figure 8. $I_{33}^{BS}(0)$ spectra of spin series PET is shown for the range of 960−1060 cm^{-1}. Curves are labeled by their respective samples. Peaks are labeled by their respective frequencies. The thin solid line is a horizontal baseline.

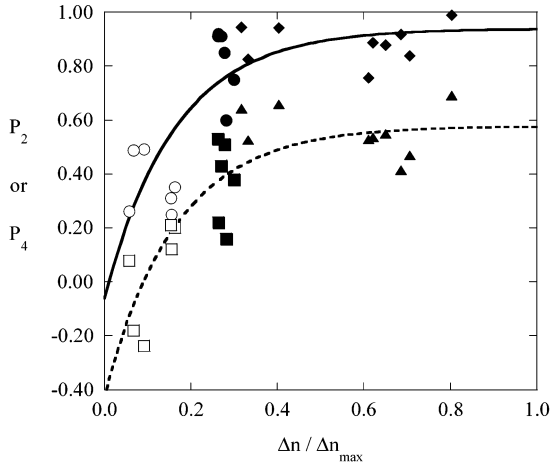

Figure 9. P_2 (● and ◆) and P_4 (■ and ▲) for the 998 cm^{-1} band and P_2 (○) and are P_4 (□) of the 993 cm^{-1} band are shown as functions of the birefringence. ●, ■, ○, and □ are for the undrawn (S-series) samples, and ◆ and ▲ are for the drawn samples. The two curves are linear regressions to the function $c + [1 - \exp(b^*\Delta n/\Delta n_{max})]$ and are provided only to guide the eye.

tion, $\Delta n = 0.045$, and low crystallinity, $X_c = 0.08$. Sample S_41 has higher orientation, $\Delta n = 0.069$, and higher crystallinity, $X_c = 0.17$. The 1030 cm^{-1} band has nearly disappeared. Both the 993 and the 998 cm^{-1} bands are increasing in strength, but the 998 cm^{-1} band is increasing more rapidly than the 993 cm^{-1} band. Heuvel[27] and Desai[28] showed that the onset of stress-oriented crystallization in PET occurs above a spinning speed of 3500 m/min. We found that sample S_32 exhibits peaks around 995 cm^{-1}, while sample S_41 exhibits a distinct peak at 998 cm^{-1}. This means that the onset of crystallization occurs between 3200 and 4113 m/min. Thus, our Raman observations are consistent with the earlier X-ray results.

Figure 9 shows P_2 and P_4 for the 993−998 cm^{-1} band as a function of the birefringence for both the undrawn (S-series) and for the drawn samples. The two curves highlight the asymptotic behavior of P_2 and P_4 as discusses in ref 21 but have no other meaning. The open points on the right side of the curve correspond to the 993 cm^{-1} band, while the solid points correspond exclusively to the 998 cm^{-1} band. This indicates that the oriented noncrystalline region (993 cm^{-1} band) is only partially oriented, whereas the crystalline region (998 cm^{-1} band) is very highly oriented. The asymptotic value for our value of P_2 for the 998 cm^{-1} band is 0.94, which is consistent with P_2 of the crystals as found by other researchers. Wide-angle X-ray scattering of a pure spin series PET by Heuvel and Huisman[27] showed that $P_{2,crystal}$ is ∼0.96. X-ray work by Desai[28] showed that the stress oriented crystallization of a pure spin speed series for $P_{2,crystal}$ is 0.89−0.93, and the polarized fluorescence study of Spruiell[29] showed that the crystal orientation is constant with $P_{2,crystal}$ just above 0.9. This is understood readily since PET crystallizes slowly *except* when oriented. The chain segments oriented by the elongation of the polymer melt crystallize many orders of magnitude faster than the unoriented chain segments.[29] Thus, the crystals are expected to be highly oriented, as observed.

Since the 998 cm^{-1} band is weak for relatively low oriented and crystallized samples, the variations in the measured values are $P_2 \pm 0.09$ and $P_4 \pm 0.12$. It was not possible to determine the ODF for this band. (For the 1616 cm^{-1} band, the variations were $P_2 \pm 0.05$ and $P_4 \pm 0.03$.) However, we can estimate the offset angle for the third principal component of the Raman tensor (α_3) of the 998 cm^{-1} band:

$$P_{2n}(\text{all-trans ethylene glycol unit}) = P_{2n}(\text{chain})\, P_{2n}(\alpha_{3,998}) \quad (14)$$

For perfect orientation, $P_{2n}(\text{chain}) = 1$. Since $P_2(\alpha_{3,998}) \geq 0.94$, $\phi \leq 12°$. Similarly, for the asymptotic value of $P_4 = 0.58$, $\phi \leq 18°$. The largest observed P_2 and P_4 values give $\phi \leq 5°$ and 15°, respectively. Thus, the angle between α_3 of the 998 cm^{-1} band and the polymer chain axis is less than or approximately 12°.

The Raman tensor ratio $a_1 = \alpha_1/\alpha_3$ is positive, is close to zero, and does not seem to depend on morphology. On the other hand, $a_2 = \alpha_2/\alpha_3$ is negative and decreases with increasing P_2 of the 998 cm^{-1} band. In addition, $\kappa\alpha_3^2 = I_0 N_0 \alpha_3^2$, where I_0 is the incident intensity and N_0 is the number of scattering centers within the

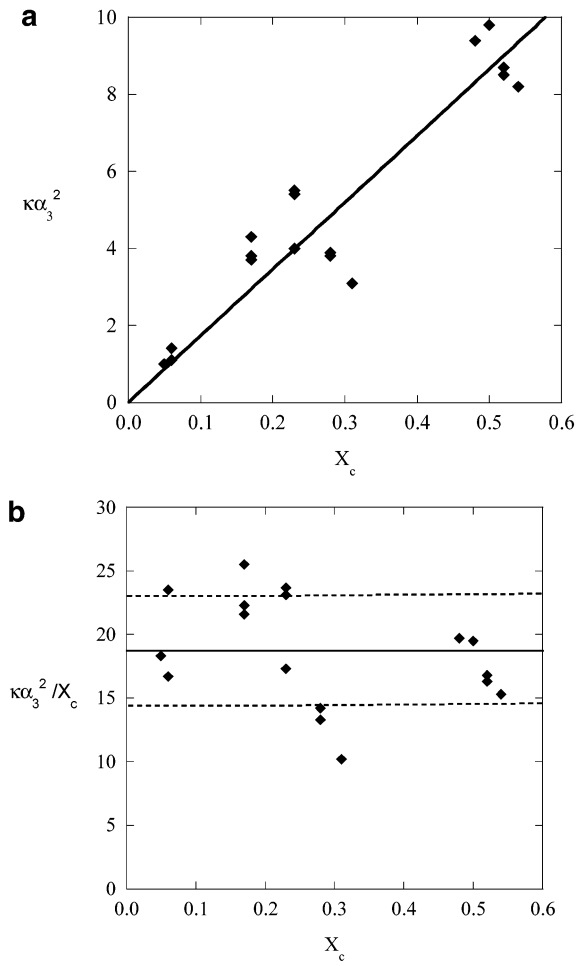

Figure 10. (a) $\kappa\alpha_3^2$ of the 998 cm^{-1} band is shown to depend linearly on the crystallinity while (b) $\kappa\alpha_3^2/X_c$ is shown to be independent of the crystallinity. The solid line is the average value, and the dashed lines are located at ±1 standard deviation. κ is an arbitrary constant.

scattering volume. $\kappa\alpha_3^2$ increases linearly with crystallinity, while $\kappa\alpha_3^2/X_c$ is independent of crystallinity (see Figure 10). This is consistent with the assignment of the 998 cm^{-1} band to the all-trans conformation of the ethylene glycol unit in the *crystalline* phase, since N_0 is directly proportional to X_c. This agrees with our previous results.[21] Thus, α_1 and α_3 are independent of morphology, which is consistent with the assumption that the local field effects are constant within the crystal. On the other hand, α_2 appears to decrease with increasing orientation. The source of this variation is difficult to understand.

Analysis of the 1096 cm^{-1} Region. The 1096 cm^{-1} region consists of bands at 1096 and 1117 cm^{-1}. The 1096 cm^{-1} band is a complicated band involving the C_1-C_4 stretch of the phenyl group, the C−O stretch of the carboxylic acid group, and the C−C stretch of the ethylene glycol unit.[12] The intensity of this band has been shown to correlate with sample density and crystallinity. We observed that its intensity increases with both the overall orientation and Lorentz density of the sample. On solving eqs 1, we found that the Raman tensor ratios of this band, a_1 and a_2, are complex numbers for all samples in the current study. In addition, $P_{2,1096}$ is substantially smaller than $P_{2,998}$. The maximum value for $P_{2,1096}$ is about 0.23 while $P_{2,998}$ is about 0.94. There is no simple relationship between the

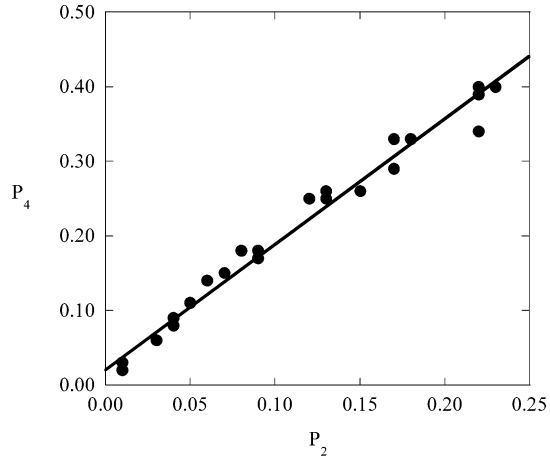

Figure 11. P_4 is shown to be linearly related to P_2 for the 1096 cm^{-1} Raman band.

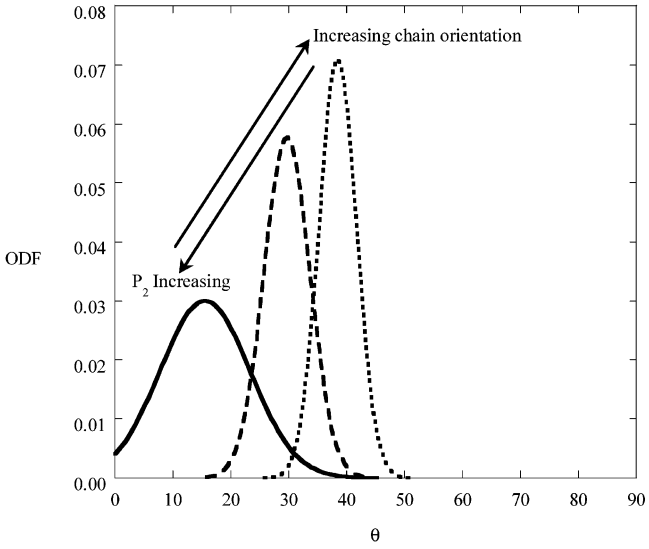

Figure 12. Orientation distribution function for the 1096 cm^{-1} Raman band is shown for $P_2 = 0.00$, dotted curve, $P_2 = 0.10$, dashed curve, and $P_2 = 0.25$, solid curve. For this band, as orientation *increases*, P_2 *decreases*.

measured values of $P_{2,998}$ and $P_{2,1096}$, even though both bands have been related to the crystal phase and both bands involve portions of the ethylene glycol unit.

Unlike the 1616 and the 998 cm^{-1} bands, P_2 and P_4 for the 1096 cm^{-1} band show no dependence on density or orientation. However, P_2 is always smaller than P_4, and there is a strong linear relationship between P_4 and P_2 for the 1096 cm^{-1} band

$$P_4 = 0.0202 + 1.685P_2 \qquad (15)$$

as shown in Figure 11. Using eqs 12, 13, and 15, we find that the orientation distribution function gets narrower and rotates to a higher angle (ϕ) as P_2 *decreases* (Figure 12).

We believe the lack of correlation between P_2 and morphology for the 1096 cm^{-1} band is due to its low intensity, that it is always overlapped with the 1117 cm^{-1} band, and the large tilt angle between α_3 and the fiber axis.

Conclusions

Polarized Raman spectroscopy in seven specific geometries was used to analyze uniaxially oriented PET

fibers. Five of these geometries are unique, and two redundant spectra are needed to normalize the five spectra to a common amplitude. The features of these spectra were used to determine the values and orientation of the principal components of the Raman tensor to the chain axis and to determine the orientation distribution functions for the 1616, 998, and 1096 cm^{-1} Raman bands as a function of processing conditions, e.g., spinning speed and draw ratio.

Our analysis of the 1616 cm^{-1} band confirmed the results of Lesko et al.,[11] showing that the Raman tensor ratios vary with morphology. We found that the two Raman tensor ratios α_1/α_3 and α_2/α_3 are of equal magnitude but opposite sign. Both change with increasing crystallinity, approaching constant values of $\alpha_1/\alpha_3 = 0.19$ and $\alpha_2/\alpha_3 = -0.19$ for highly crystalline samples. The square of the third principal component of the Raman tensor, α_3^2, increases with crystallinity. We also found that both P_2 and P_4 increase monotonically with birefringence. By assuming a Gaussian distribution of chain orientation with an angular offset, we obtained orientation distribution functions (ODFs) for α_3(1616). For low-birefringence samples, ODF for the C_1-C_4 axis is nearly flat. As the birefringence increases, the ODF first begins to peak around 0°, but at high birefringence and high crystallinity, the ODF narrows and rotates to 23°. Daubeny and Bunn[26] found that, in the crystalline phase, the C_1-C_4 axis lies at 23° to the chain axis. Purvis and Bower[3] assumed that the C_1-C_4 axis lies at 19° to the chain axis in their model of the normal modes of crystalline PET and that α_3 was collinear with the C_1-C_4 axis. The results of the present study indicate that the α_3 axis is nearly collinear with the C_1-C_4 axis of the benzene ring in PET, as assumed by Purvis and Bower.[3]

Our analysis of the 998 cm^{-1} band agrees with the assignment of this band to the all-trans conformation of the glycol unit in crystalline PET.[13] We found that the crystal orientation, $P_{2,998}$, is nearly constant at a value of ~0.94 for all samples in which the 998 cm^{-1} band could be seen. After the onset of stress-oriented crystallization, the increase of the orientation of the crystals is small. P_2 of the 993 cm^{-1} band is larger than the average chain orientation but much smaller than P_2 of the 998 cm^{-1} band. This is consistent with the assignment of the 993 cm^{-1} band to the all-trans conformation of the ethylene glycol unit in the noncrystalline region.[13] The Raman tensor ratio α_1/α_3 of the 998 cm^{-1} band is positive, close to zero, and independent of crystallinity or orientation. The α_3 principal component of the Raman tensor is also independent of crystallinity and orientation. These results indicate that the local field effect within the crystals is uniform and is consistent with the assignment of the 998 cm^{-1} band to the crystalline phase. The Raman tensor ratio α_2/α_3 is negative and decreases with increasing crystal orientation, which is difficult to explain. The analysis of P_2 and P_4 indicates that α_3(998) is aligned close to the fiber axis in the fibers used in this study, $\phi \leq 12°$.

Although the 1096 cm^{-1} Raman band has also been assigned to the crystalline region, P_2 of the 1096 cm^{-1} band is substantially smaller than for the 998 cm^{-1} band. In addition, P_4 of the 1096 cm^{-1} band is always larger than P_2. The orientation parameters P_2 and P_4 have a linear relationship with each other. Again using a Gaussian distribution for α_3 of the 1096 cm^{-1} band with an offset angle relative to the fiber axis, we found that this band always has a narrow distribution with a large tilt angle. As the fiber orientation increases, the tilt angle increases and the distribution becomes narrower.

These results show that polarized Raman spectroscopy can be a very powerful tool for making detailed measurements of the morphology of cylindrically symmetric fibers.

Acknowledgment. The authors thank the National Textile Center (NTC), Department of Commerce, for funding this research and Drs. Prashant Desai and Edgar Rudisill for providing the polyester samples.

References and Notes

(1) Bower, D. I. *J. Polym. Sci., Polym. Phys. Ed.* **1972**, *10*, 2135−2153.
(2) Purvis, J.; Bower, D. I.; Ward, I. M. *Polymer* **1973**, *14*, 398−400.
(3) Purvis, J.; Bower, D. I. *J. Polym. Sci., Polym. Phys. Ed.* **1976**, *14*, 1461−1484.
(4) Nobbs, J. H.; Bower, D. I.; Ward, I. M. *J. Polym. Sci., Polym. Phys. Ed.* **1979**, *17*, 259−272.
(5) Jarvis, D. A.; Hutchinson, I. J.; Bower, D. I.; Ward, I. M. *Polymer* **1980**, *21*, 41−54.
(6) Bower, D. I.; Jarvis, D. A.; Ward, I. M. *J. Polym. Sci., Polym. Phys. Ed.* **1986**, *24*, 1459−1479.
(7) Bower, D. I.; Jarvis, D. A.; Lewis, E. L. V.; Ward, I. M. *J. Polym. Sci., Polym. Phy.* **1986**, *24*, 1481−1492.
(8) Bower, D. I.; Ward, I. M. *Polymer* **1982**, *23*, 645−649.
(9) Lapersonne, P.; Bower, D. I.; Ward, I. M. *Polymer* **1992**, *33*, 1266−1276.
(10) Everall, N. J. *Appl. Spectrosc.* **1998**, *52*, 1498−1504.
(11) Lesko, C. C. C.; Rabolt, J. F.; Ikeda, R. M.; Chase, B.; Kennedy, A. *J. Mol. Struct.* **2000**, *521*, 127−136.
(12) Boerio, F. J.; Bahl, S. K. *J. Polym. Sci., Polym. Phys. Ed.* **1976**, *14*, 1029−1046.
(13) Stokr, J.; Schneider, B.; Doskocilova, D.; Lovy, J. *Polymer* **1982**, *23*, 714−721.
(14) Everall, N.; Tayler, P.; Chalmers, J. M.; MacKerron, D. *Polymer* **1994**, *35*, 3184−3192.
(15) Quintanilla, L.; Rodriguez-Cabello, J. C.; Pastor, J. M. *J. Raman Spectrosc.* **1994**, *25*, 335−344.
(16) Adar, F.; Noether, H. *Polymer* **1985**, *26*, 1935−1943.
(17) Ellis, G.; Roman, F.; Marco, C.; Gomez, M. A.; Fatou, J. G. *Spectrochim. Acta, Part A* **1995**, *51*, 2139−2145.
(18) Adar, F.; Noether, H. *SPIE* **1992**, *1636*, 42−52.
(19) McGraw, G. E. In *Polymer Characterization Interdisciplinary Approaches;* Craver, C. D., Ed.; Plenum Press: New York, 1971.
(20) Citra, M. J.; Chase, D. B.; Ikeda, R. M.; Gardner, K. H. *Macromolecules* **1995**, *28*, 4007−4012.
(21) Yang, S.; Michielsen, S. *Macromolecules* **2002**, *35*, 10108−10113.
(22) Natarajan, S. Characterization of Poly(ethylene terephthalate) Fibers Using Raman Microscopy. Master Thesis, Georgia Institute of Technology, 1998.
(23) Yang, S. Analysis of Poly(ethylene terephthalate) Fibers Using Polarized Raman Microscopy. PhD Thesis, Georgia Institute of Technology, 2002.
(24) Natarajan, S.; Michielsen, S. *J. Appl. Polym. Sci.* **1999**, *73*, 943−952.
(25) Rule, M. In *Polymer Handbook*; Brandrup, J., Immergut, E. H., Grulke, E. A., Eds.; John Wiley and Sons: New York, 1999; p V113.
(26) Daubeny, R. de P.; Bunn, C. W. *Proc. R. Soc. London* **1954**, *A226*, 531−542.
(27) Heuvel, H. M.; Huisman, R. *J. Appl. Polym. Sci.* **1978**, *22*, 2229−2243.
(28) Desai, P. Fundamental Aspects of Crystallization and Thermorheological Behavior of Uniaxially Oriented Polymers. PhD Thesis, Georgia Institute of Technology, 1988.
(29) Spruiell, J. E. In *Structure Formation in Polymeric Fibers*; Salem, D. R., Ed.; Hanser Gardner Publications: Cincinnati, OH, 2001; pp 53−55.

MA034486Q